3rd International Conference on Advances in Civil and Environmental Engineering (ICACEE-2024)

University of Engineering & Technology Taxila, Pakistan

Conference dates: 21st and 22nd February 2024; ISBN: 978-969-23675-2-3

Finite Element Simulations of Retrofitted Recycled Aggregate Concrete Columns Having FRP Bars

Raja Tufail Hussain Khan[1], Muhammad Abbas Ali[1,*], Shahir Ahmad Safi[1], Ali Raza[1], Muhammad Arshad[1]

[1]Department of Civil Engineering, University of Engineering and Technology Taxila, 47050, Pakistan

*Corresponding author: 20-ce-183@students.uettaxila.edu.pk

ABSTRACT

Glass fiber reinforced polymer (GFRP) rebars offer a durable alternative to steel in harsh environments. This study assesses a fast repair method for partially damaged recycled aggregate geopolymer concrete (RAGC) elements with GFRP reinforcement. It compares 9 repaired elements combining experimental techniques and finite element analysis (FEA). The rapid repair involves carbon fiber-reinforced polymer (CFRP) wraps. The research examines how exterior CFRP confinement affects failure modes, ultimate axial load, and axial deflection. FEA samples predict axial behavior accurately. Both experimental and FEA results consistently show that the rapid repair method significantly restores ultimate axial load and axial deflection capacities in pre-damaged RAGC elements.

KEYWORDS: Recycled aggregate; retrofitting; finite element analysis; cfrp wraps; GFRP bars

1. INTRODUCTION

Fiber-reinforced polymer (FRP) has developed as an advanced composite material in the construction industry, showing promise in both new structures and the rehabilitation of existing ones. FRP composites offer distinct advantages, primarily enhancing the durability and energy absorption competence of structures. They are also effective in resisting crack propagation, fatigue loads, shocks, and corrosion [1, 2]. FRP rebars are widely used in various concrete structures, including tunnels, water tanks, seawalls, and parking garages [3, 4].

For retrofitting and repairing structures with both slight and extensive damage, numerous studies are available, encompassing FRP jacketing, concrete utilization, and the adoption of steel to restore ductility and capacity in damaged reinforced elements [5-7]. However, the most prevalent approach among these techniques is the jacketing of concrete elements with FRP composites. Conversely, when undertaking repair, it is essential to maintain the original sizes of structural members. Thus, the installation of FRP wraps around columns proves to be the most effective techniques [8].

On the contrary, in comparison to the 12% contribution of steel rebars, another study suggested a 10% contribution of GFRP rebars to enhance the element's capacity [9]. Consequently, this research recommends the utilization of GFRP reinforcing for elements with adequate confinement. Mohamed et al. assessed the behavior of longitudinally wrapped CFRP and GFRP concrete

elements, revealing corresponding strains of 0.004 and 0.007 mm/mm for FRP rebars. Hence, it is claimed that due to the efficiently sourced reinforcing from FRP, wrapped compression members exhibit enhanced load-carrying capacities in elements [10]. Elmessalami et al. [11] disclosed that, in comparison to steel-reinforced elements, incorporating FRP reinforcement in concrete elements exhibited 7-8% less capacity at the same axial stiffness, indicating similar performance of both elements in compression. Afifi et al. [12] examined the ductility indices of GFRP rebars in wrapped circular concrete elements. Based on the utilized GFRP reinforcing ratio and the degree of confinement, researchers observed a variance range of 1.19-4.75.
Many studies highlight the potential of GFRP rebars as a steel alternative in compression-loaded reinforced concrete. However, there's a lack of research on pre-damaged GFRP-reinforced RAGC elements repaired with FRP wraps. This study fills this gap by experimentally and numerically analyzing how eccentric and concentric loads affect pre-damaged GFRP-reinforced RAGC elements. The original samples sustained compression damage, reducing axial capacity by up to 35% post-ultimate. The repairing process used CFRP wraps. The proposed numerical sample is validated against experimental results. This study focuses on rehabilitating FRP-wrapped and reinforced elements, aiming to understand FRP retrofitting behavior and develop a recovery philosophy for damaged elements.

2. EXPERIMENTAL SETUP

2.1.Materials

Recycled aggregate geopolymer concrete (RAGC) was prepared by replacing natural aggregates with recycled ones. Recycled coarse aggregates (RCA) from 12 months old concrete cylinders (30-45 MPa) were used. A maximum size of 10 mm was used for coarse aggregates. Lawrancepur sand (2586 kg/m^3, fineness modulus 2.25) was locally sourced. Granular analyses are in Figure 1. The mix included ViscoCrete®-3425 superplasticizer for workability. Table 1 guided the mix design based on RCA water absorption. The nominal density was 2,400 kg/m^3. RAGC used 55% GGBS and 45% class F fly ash. An activator mix of Na_2SiO_3 and 14 M NaOH (1:2.5) was employed. The fresh RAGC had a 125 mm slump, tested per ASTM C143-15. The setting time was 90 minutes per ASTM C807-13. The 28-day compressive strength of 150 mm diameter, 300 mm height specimens was 30.5 MPa. All six compression test cylinders came from the same mix.

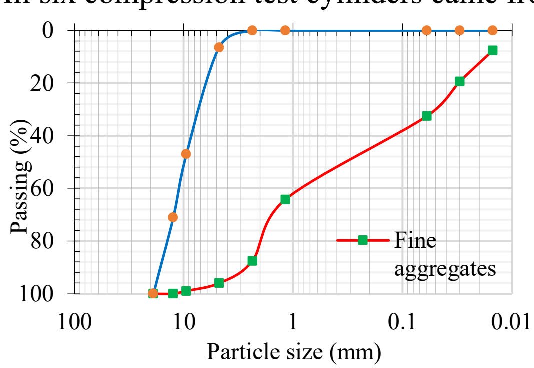

Figure 1: Granulometric analysis (a) fine aggregates (b) RCA

Table 1: Mix design of RAGC

Material	Quantity (kg/m^3)	Material	Quantity (kg/m^3)
Fly ash	246	RCA	1184
Sand	498	NaOH solution	38
Water	120	Superplasticizer	39
GGBS	165	Na_2SiO_3	106

2.2.Repairing and Testing Technique

Nine cylindrical specimens composed of reactive powder concrete (RPC) were fabricated, each measuring 1200 mm in height and 300 mm in cross-sectional diameter (see Table 2). All specimens were reinforced with both GFRP ties and rebars. The GFRP-reinforced RPC specimens featured transverse and longitudinal reinforcement with diameters of 12 mm and 19 mm, respectively. Some specimens were intentionally left partially damaged and unrepaired to study the behavior of repaired GFRP-reinforced samples. Repairs included cementitious grouting, epoxy injection, and wrapping with CFRP wraps. Visual inspection revealed varying damage levels under different loading conditions. To rectify permanent deformations, partially damaged GFRP were straightened, and loose concrete was removed using chisel head hammers. The surface was cleaned with steel wire brushes and compressed air. Chemical bonding was achieved using CHEMDUR-31. Two grouts—mortar grout for heavily damaged areas and cementitious grout for slightly damaged areas—were developed. Epoxy-impregnated thick mortar grout and high-performance cementitious grout were used for repair. After concrete repair, the samples were ground and primed with epoxy resin. CFRP wraps were applied and coated with epoxy resin. Superplasticizer was used to reduce fabric voids and enhance bonding. CFRP fabric was overlapped to prevent failure, and the samples were cured 10 days before final testing. Figure 2 shows the testing arrangement for eccentrically loaded members.

Table 2: Test samples

Sample ID	Main rebars		Transverse rebars			Eccentricity (mm)	Eccentricity to diameter ratio
	Bar number & diameter	Ratio (%)	Diameter (mm)	Spacing (mm)	Ratio (%)		
75-0-GRAGC	6-19 mm	2.40	12.0	75	1.880	0	000
75-30-GRAGC	6-19 mm	2.40	12.0	75	1.880	30	0.10
75-60-GRAGC	6-19 mm	2.40	12.0	75	1.880	60	0.20
150-0-GRAGC	6-19 mm	2.40	12.0	150	0.940	0	000
150-30-GRAGC	6-19 mm	2.40	12.0	150	0.940	30	0.10
150-60-GRAGC	6-19 mm	2.40	12.0	150	0.940	60	0.20
250-0-GRAGC	6-19 mm	2.40	12.0	250	0.660	0	000
250-30-GRAGC	6-19 mm	2.40	12.0	250	0.660	30	0.10
250-60-GRAGC	6-19 mm	2.40	12.0	250	0.660	60	0.20

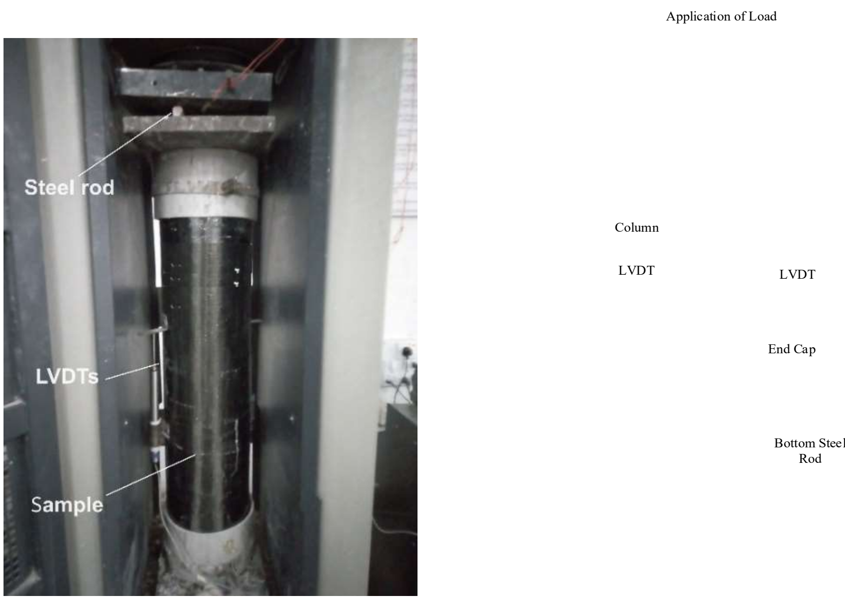

(a) (b)

Figure 2: Testing arrangement for eccentrically loaded element (a) experimental setup (b) schematic diagram

3. DISCUSSION OF RESULTS

3.1.Load-deflection curves

Figure 3 shows load-deflection curves for both original (denoted as O) and repaired (denoted as R) samples. For example, 75-0-GRAGC(R) represents the behavior of concentrically loaded GFRP-reinforced samples after retrofitting with CFRP. Repaired samples showed improved axial capacities and deflections, fully recovering their strengths. Loading regimes, reinforcing spacing, and main bars significantly influenced the failure mode. Primarily, strengthened samples failed due to CFRP ruptures and de-bonding, with subsequent concrete cracks. However, the CFRP-concrete interface remained intact, while the weaker cover-core interface failed. All repaired elements suffered from CFRP rupture and de-bonding, but no interfacial failure was reported due to effective bonding. GFRP-reinforced RAGC samples exhibited differences between concentric and eccentric loading, with smaller tie spacing resulting in increased axial deflections due to better energy absorption. Failure modes varied, with cracks on the concrete surface, rupturing and debonding of CFRP, and global buckling leading to element failure.

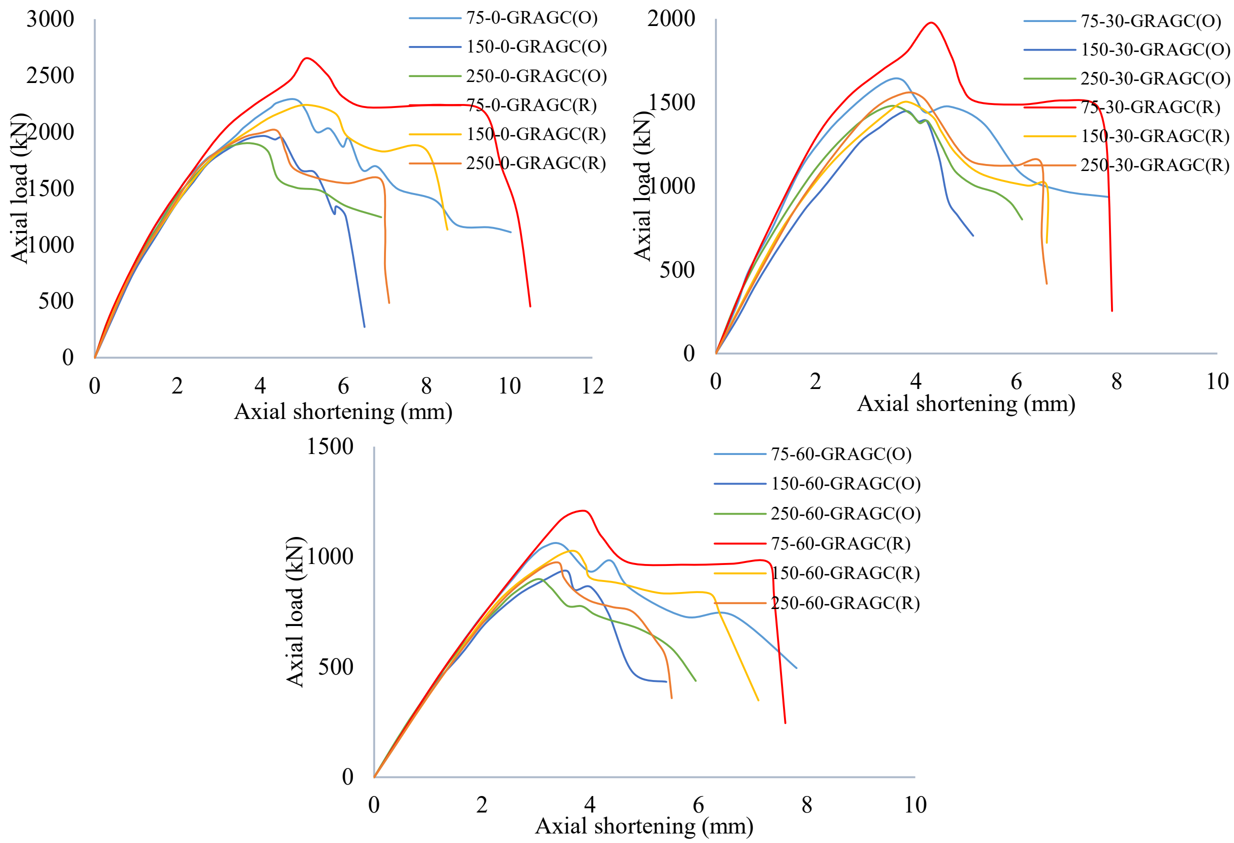

Figure 3: Comparison of axial load-deflection curves of original and repaired members

3.2.Ultimate Axial Load

Post-repair, both concentrically and eccentrically loaded samples fully restored their axial strength. Uniaxial eccentric loading led to full recovery of deflection and maximum axial strength in GFRP-reinforced RAGC members. CFRP wraps were effective in bending-dominant loadings, slightly reducing axial stiffness in GFRP-reinforced samples. Lateral confinement was made possible by external CFRP bonding that decreased abrupt debonding in the transverse direction. As a result, the concrete core was effectively encased, increasing its axial load capacity and energy absorption. As a result, the ultimate strength and axial deflection were fully recovered. In comparison to the original samples, Figure 4 illustrates the enhanced ultimate load-carrying potential of the restored parts. RAGC members reinforced with GFRP recovered by 9.65% on average. This discrepancy could be the result of less damage to the transverse rebars during testing.

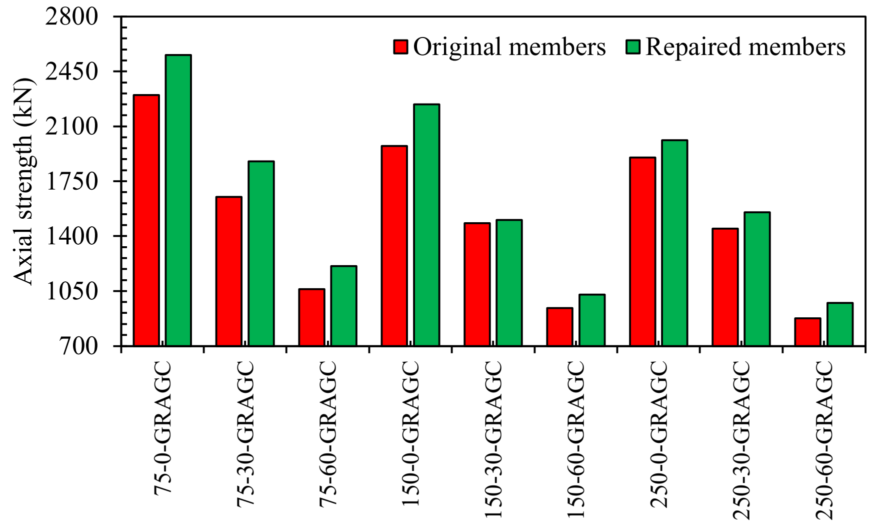

Figure 4: Comparison between the ultimate axial load of RAGC elements before and after repairing

4. FINITE ELEMENT MODELING

The ABAQUS 6.14 commercial software package was employed for the extended FEM analysis of the RAGC element members. Using the experimental data, a reference sample (75-0-GRAGC) was validated for FEM-based estimates. Consistent with previous suggestions [13, 14], GFRP rebars were modeled with deformable truss elements, while deformable stress elements were used to sample RAGC. Linear elastic and bilinear elastoplastic samples were employed to define GFRP rebars, respectively. Additionally, a prevalent concrete damaged plasticity (CDP) modeling approach was fine-tuned to adjust certain plastic constraints of RAGC, as recommended earlier [15, 16].

All degrees of freedom were kept free for translation but restrained for rotation. Moreover, the deflection restraint approach was utilized to apply uniform compression at the top end. The restraint of the 'embedded vicinity' linked the necessary DOF of GFRP truss elements with the desired DOFs of RAGC. The available constraints for delineating the embedded region were utilized to define the bond existing between GFRP rebars and RAGC [15, 16]. Figure 5 illustrates the FEM simulations of the sample. To determine the compressive stress and strain of FRP-confined concrete Eq. (1) and Eq. (2) were used.

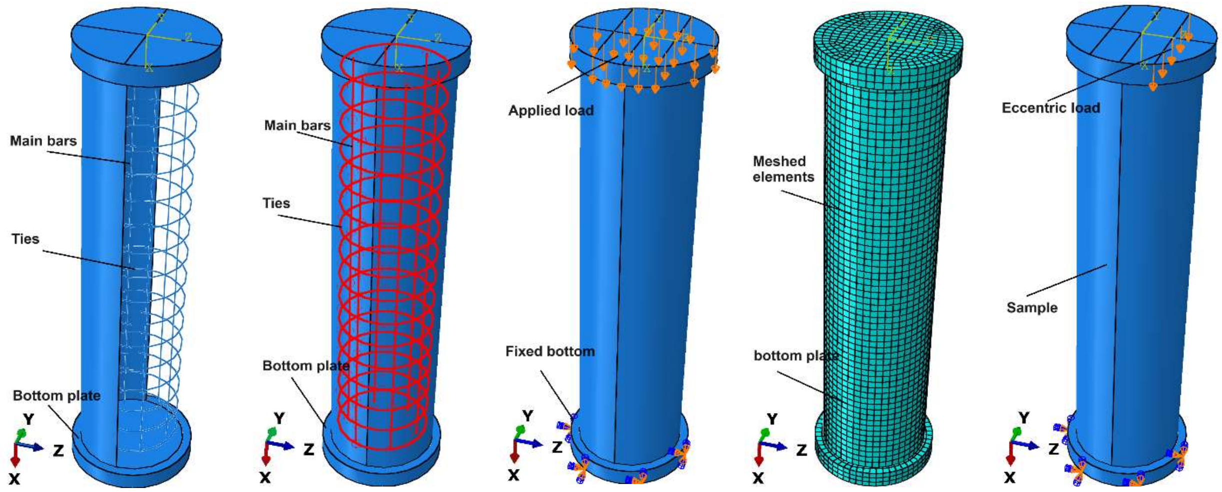

(a) (b) (c) (d) (e)

Figure 5: FEA simulation of elements (a) geometry (b) embedded region (c) applied concentric load (d) meshing of sample (e) applied eccentric load

$$\frac{f'_{cc}}{f'_{co}} = 1.0 + 4.547\left(\frac{f_{le}}{f'_{co}}\right)^{0.723} \tag{1}$$

$$\frac{\varepsilon'_{cc}}{\varepsilon'_{co}} = 1.0 + \left(\frac{0.024}{\varepsilon'_{co}}\right)\left(\frac{f_{le}}{f'_{co}}\right)^{0.907} \tag{2}$$

Here f_{le} is the effective confinement strength presented by Eq. (6) [17].

$$f_{le} = \frac{2E_f \varepsilon_{h,rup} t}{D} \tag{3}$$

Here, E_f is the elastic modulus, $\varepsilon_{h,rup}$ is the hoop rupture strain, and 't' is the thickness/diameter of the ties. The tension damage parameter (d_t) and the compression damage parameter (d_c) are utilized to define the damages in RAGC. The compression strength of RAGC (σ_c), the tensile strength of RAGC (σ_t) d_c, and d_t is presented as below (refer to Eq. (4-7):

$$\sigma_c = (1 - d_c)E_o\left(\varepsilon_c - \varepsilon_c^{pl}\right) \tag{4}$$

$$\sigma_t = (1 - d_t)E_o\left(\varepsilon_t - \varepsilon_t^{pl}\right) \tag{5}$$

$$d_c = \frac{1}{e^{-1/m_c} - 1}\left(e^{-\varepsilon_{c,norm}^{in}/m_c} - 1\right) \tag{6}$$

$$d_t = \frac{1}{e^{-1/m_t} - 1}\left(e^{-\varepsilon_{t,norm}^{ck}/m_t} - 1\right) \tag{7}$$

For GFRP rebars, the Poisson's ratio was established as 0.25 [18]. The material behavior of GFRP rebars up to the point of rupture is characterized using an elastic model with a linear relationship.

The "LAMINA" material type was used to model the elastic behavior of CFRP wraps. According to Liu et al. [19], the material's elastic modulus in the transverse direction (E_1) was 231 GPa, and E_2, G_{12}, G_{13}, and G_{23} were assigned a small portion of the elastic properties in the fiber direction [20]. A 0.30 Poisson's ratio was utilized. A tensile strength of 4100 MPa in the fiber direction was used to simulate the failure stresses in the sub-options of the elastic model.

Figure 6 compares the test and FEA load-deflection curves for the control sample. The FEM of 75-0-GRAGC showed a 5.44% difference in ultimate axial load and a 1.96% difference in associated deflection compared to experimental results, indicating a satisfactory level of accuracy. Discrepancies could stem from real-world versus simulated conditions, ingredient strengths, casting imperfections, bar properties, and assumptions about the bond between RAGC and rebars. Despite these, the FEM closely correlates with testing, promising further examination of GRAGC and SRAGC elements.

The highest difference in axial strength, 11.26%, occurred in the 250-30-SRAGC sample, while for axial deflection at ultimate load, it was 26.7% in the 75-30-SRAGC sample. Variations may stem from initial geometric differences not fully considered in FEM. While FEM was validated with GRAGC, it accurately estimated SRAGC behavior for strength and deflection. On average, differences were 4.2% and 7.0% for ultimate axial load, rising to 7.5% and 9% for axial deflection under ultimate load for GRAGC and SRAGC samples, respectively. For eccentric loading, FEM simulations yielded satisfactory axial strength values with errors of 4.6% and 6.1% for concentric and eccentric loading, respectively. This suggests well-defined behavior under tensile stresses. The proposed FEM can accurately estimate axial capacity for GRAGC and SRAGC elements. Figure 7 shows the percentage deviation between experimental and FEA ultimate axial load predictions for all samples. ABAQUS simulations consistently displayed an average discrepancy of 5.6% for axial ultimate load and 8.3% for associated axial deflection. The 250-30-SRAGC sample had the highest error. Overall, ABAQUS provided a close approximation to experimental outcomes, with discrepancies within an acceptable range, reinforcing FEA's reliability in capturing essential behavior.

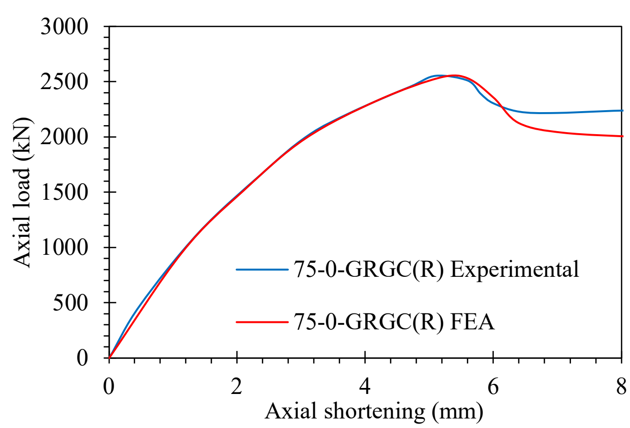

Figure 6: Test versus FEA load-deflection curves for the control sample

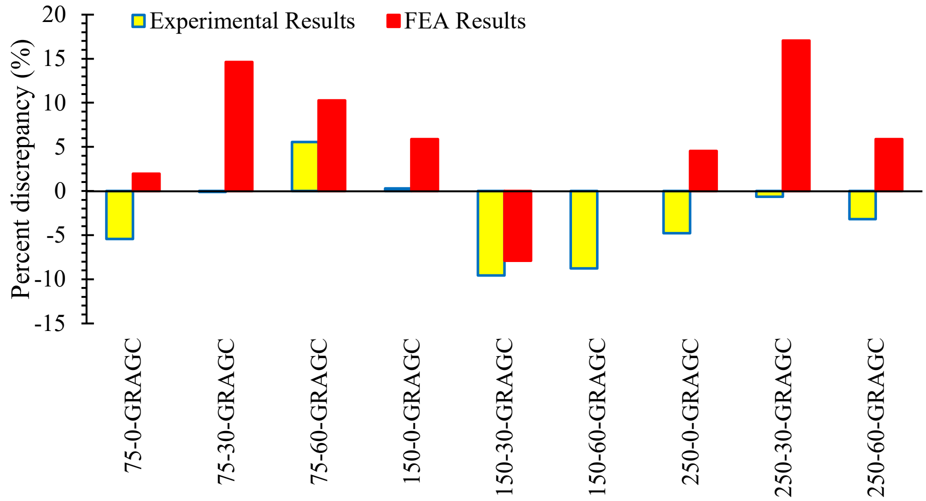

Figure 7: The percent difference between test results and FEA simulations for the ultimate axial load of all studied samples

5. CONCLUSION

The following conclusions can be drawn from present research:

- The application of RAGC-enriched axial loads and structural behavior in both GFRP-reinforced RAGC elements makes it a viable option for realistic applications in engineering. Effective external confinement is crucial for ensuring its success in RAGC elements and contributes to ecological development practices.
- The proposed rapid repair methodology effectively restored complete strength in GFRP-reinforced RAGC samples under axial compressive loads, demonstrating similar ultimate axial load recovery in GFRP-reinforced samples under higher eccentricity loads.
- The RAGC-based CDP sample, which was used to create the suggested FEA sample, effectively captured the complicated structural response of repaired RAGC elements. The minimal discrepancies were found in the axial load and corresponding axial deflection, at 5.6% and 8.3%, respectively. The FEA sample's outstanding correctness validates its application in the GRAGC members' parametric analysis.

Acknowledgments
None.

References

1. Mehta, P.K. and P.J. Monteiro, *Concrete: microstructure, properties, and materials*. 2014: McGraw-Hill Education.
2. Bentur, A. and S. Mindess, *Fibre reinforced cementitious composites*. 2006: Crc Press.
3. Benmokrane, B., et al. *Design, construction, and monitoring of the first worldwide two-way flat slab parking garage reinforced with GFRP bars*. in *Proc., 6th Int. Conf. on FRP Composites in Civil Engineering*. 2012.

4. Benmokrane, B. and H.M. Mohamed, *Extending the service life of water treatment structures.* Concrete international, 2014. **36**(2): p. 40-45.
5. Manalo, A.C., et al., *Investigation into fibre composites jacket with an innovative joining system.* Construction and Building Materials, 2014. **65**: p. 270-281.
6. Mohammed, A.A., et al., *Behavior of damaged concrete columns repaired with novel FRP jacket.* Journal of Composites for Construction, 2019. **23**(3): p. 04019013.
7. Zhao, X.-L. and L. Zhang, *State-of-the-art review on FRP strengthened steel structures.* Engineering structures, 2007. **29**(8): p. 1808-1823.
8. Ilki, A. and N. Kumbasar, *Behavior of damaged and undamaged concrete strengthened by carbon fiber composite sheets.* Structural Engineering and Mechanics, 2002. **13**(1): p. 75-90.
9. Tobbi, H., A.S. Farghaly, and B. Benmokrane, *Concrete Columns Reinforced Longitudinally and Transversally with Glass Fiber-Reinforced Polymer Bars.* ACI Structural Journal, 2012. **109**(4).
10. Mohamed, H.M., M.Z. Afifi, and B. Benmokrane, *Performance evaluation of concrete columns reinforced longitudinally with FRP bars and confined with FRP hoops and spirals under axial load.* Journal of Bridge Engineering, 2014. **19**(7): p. 04014020.
11. Elmessalami, N., A. El Refai, and F. Abed, *Fiber-reinforced polymers bars for compression reinforcement: A promising alternative to steel bars.* Construction and Building Materials, 2019. **209**: p. 725-737.
12. Afifi, M.Z., H.M. Mohamed, and B. Benmokrane, *Strength and axial behavior of circular concrete columns reinforced with CFRP bars and spirals.* Journal of Composites for Construction, 2014. **18**(2): p. 04013035.
13. Raza, A., and Umer Rafique., *Efficiency of GFRP Bars and Hoops in Recycled Aggregate Concrete Columns: Experimental and Numerical Study.* Composite Structures 2020: p. 112986.
14. Raza, A., et al., *Finite element modelling and theoretical predictions of FRP-reinforced concrete columns confined with various FRP-tubes.* Structures, 2020. **26**: p. 626-638.
15. Raza, A., Khan, QuZ,. Ahmad, A., *Reliability analysis of proposed capacity equation for predicting the behavior of steel-tube concrete columns confined with CFRP sheets.* Computers and Concrete, 2020. **25**(5): p. 383-400.
16. Raza, A., et al., *Structural performance of FRP-RC compression members wrapped with FRP composites.* Structures, 2020. **27**: p. 1693-1709.
17. Raza, A., Shah, SAR., Khan, AR., Aslam, MA., Khan, TA., Arshad, K., Hussan, S., Sultan, A., Shahzadi, G., Waseem, M., *Sustainable FRP-Confined Symmetric Concrete Structures: An Application Experimental and Numerical Validation Process for Reference Data.* Applied Sciences, 2020. **10**(1): p. 333.
18. Elchalakani, M., Karrech, A., Dong, M., Ali, MSM., Yang, B., *Experiments and finite element analysis of GFRP reinforced geopolymer concrete rectangular columns subjected to concentric and eccentric axial loading.* Structures, 2018. **14**: p. 273-289.
19. Liu, J.-P., et al., *Axial behaviour of circular steel tubed concrete stub columns confined by CFRP materials.* Construction Building Materials, 2018. **168**: p. 221-231.

20. Sharif, A.M., G.M. Al-Mekhlafi, and M.A. Al-Osta, *Structural performance of CFRP-strengthened concrete-filled stainless steel tubular short columns.* Engineering Structures, 2019. **183**: p. 94-109.